Multilevel rate-equation analysis to explain the recent observations of limitations to optical limiting dyes

Steve Hughes* and Brian Wherrett

Department of Physics, Heriot-Watt University, Edinburgh EH14 4AS, United Kingdom

(Received 10 October 1995; revised manuscript received 24 June 1996)

A theoretical rate-equation analysis is presented to investigate the molecular properties that are important for achieving high-fluence optical limiting. Critical conditions for achieving induced absorption are derived in terms of the material and laser parameters by employing a range of hierarchical energy-level models. The influences of stimulated emission and saturation of the excited-state absorption are seen to induce the regime of optical limiting to one of increasing transmittance. This is in direct agreement with recent experimental measurements. [S1050-2947(96)04110-8]

PACS number(s): 42.55.Mv, 32.80.Rm, 33.80.Rv, 42.65.−k

I. INTRODUCTION

At high incident radiation fluences the buildup of population in an excited state leads to a reduction or an increase of the corresponding absorption coefficient. The latter response is referred to as reverse saturable absorption (induced absorption) for dyes, and since it is associated with electronic transitions it can be extremely fast. Consequently, there have been proposals for its application to laser mode locking [1], short-pulse optical limiting [2–8], and optical bistability [9]. Such behavior was described by Giuliano and Hess [10], who noticed that the absorption of certain dyes increased with increasing irradiance (induced absorption).

For reverse saturable absorption (RSA), absorption by suitable photons excite molecules into a higher-lying energy state, whereby the excited-state species absorbs photons at a rate that is greater than that of the ground-state species, and strong optical limiting may be achieved. In the literature [1,2,11,12,9,13] RSA dyes are defined as those materials having a larger excited-state cross section σ_{21} than the ground-state absorption cross section σ_{10}. It has therefore been common to define the critical condition for the achievement of RSA to be $R>1$, where $R=\sigma_{21}/\sigma_{10}$. This criterion originates from taking a steady-state model for the classic RSA three-level energy diagram as depicted in Fig. 1(a).

Recently, it is has been demonstrated for picosecond pulses that the regime of reverse saturable absorption is not solely wavelength dependent and there is a limit to the dynamic range for induced absorption [14–16], even for very large R values. In this respect, saturation of the excited-state absorption, and hence the RSA, occurs. The purpose of this paper is to gain some insight into the basic physical mechanisms that lead to this limitation by utilizing a continuous-wave (steady-state) and dynamic rate-equation analysis. The basic three-level model is extended to incorporate effects such as stimulated emission and saturation of the excited-state absorption, and modified critical conditions are obtained for achieving optical limiting in terms of the material

and radiation parameters. These results are important for explaining recent experimental findings, predicting trends between materials, as well as enabling ''device'' figures of merit to be satisfied.

II. THEORETICAL MODELS

Figures 1(a)–1(d) indicate schematically the energy-level models to be employed and the proposed parameters (absorption cross sections σ_{ji} and lifetimes τ_{ij}) that will determine the form of the coupled rate equations, whose solution is sought to describe the RSA process. The first radiatively coupled excitation is the $S_0{\rightarrow}S_1$ transition, which is itself radiatively coupled to S_2. The labeled subscripts ($|0\rangle,|1\rangle,|2\rangle,|3\rangle$) have been chosen for simplicity, but in practice these levels may be embedded in a spectra of singlet and triplet states coupled nonradiatively or via spontaneous emission to the ground state.

The S_i label the electronic energy levels of the associated singlet manifold and the vibrational and rotational levels therein and the N_i denote the molecular population densities of the associated levels. Since the analysis is of interest for
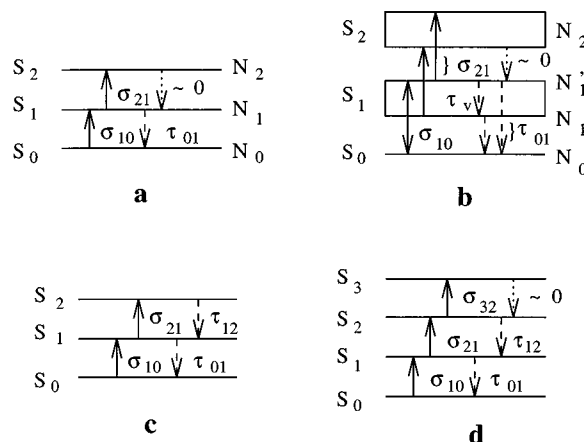
FIG. 1. Energy-level molecular models used for the rate equation analysis, showing various singlet (S_i) manifolds and, schematically, radiative absorption and stimulated emission processes and intramanifold and intermanifold recombination.

*Present address: Department of Physics, University of Tokyo, 7-3-1 Hongo, Bunkyo-Ku, Tokyo 113, Japan.

ultrafast (picosecond) pulses, the triplet states can essentially be neglected because even for heavy-metal phthalocyanines, intersystem crossing times are typically nanoseconds [3].

Consider the expression below for nonlinear absorption

$$\alpha_{nl} = N_0\sigma_{10} + N_1\sigma_{21}, \tag{1}$$

which can be written

$$\frac{\alpha_{nl}}{\alpha_0} = 1 + \frac{N_1}{N_T}(R-1), \tag{2}$$

where α_0 is the low irradiance (linear) absorption coefficient and N_T is the total molecular population density. For increasing incident irradiances, optical limiting occurs when the absorption cross section of the excited species is sufficiently larger than that of the ground-state species [i.e., the $N_1\sigma_{21}$ contribution becomes significantly large in Eq. (1)]. It is noteworthy that the condition for accomplishing induced absorption is $R > 1$, irrespective of the irradiance.

From the energy-level diagram, one can construct rate equations to describe the changes in populations and irradiance. For example, consider the case for Fig. 1(a), which is the model used by most groups [2,17,18,4,19–21]:

$$\dot{N}_0 = -N_0\sigma_{10}\frac{I}{\hbar\omega} + \frac{N_1}{\tau_{01}}, \tag{3}$$

$$\dot{N}_1 = N_0\sigma_{10}\frac{I}{\hbar\omega} - \frac{N_1}{\tau_{01}} - N_1\sigma_{21}\frac{I}{\hbar\omega} + \frac{N_2}{\tau_{12}}, \tag{4}$$

$$\dot{N}_2 = N_1\sigma_{21}\frac{I}{\hbar\omega} - \frac{N_2}{\tau_{12}}, \tag{5}$$

$$\frac{1}{c}\frac{\partial I}{\partial t} + \frac{\partial I}{\partial y} = -I[N_0\sigma_{10} + N_1\sigma_{21}], \tag{6}$$

where I is the irradiance, ω is the frequency of the laser light, and y is the direction of propagation. Note that the rate-equation approximation is valid here since for the maximum irradiances to be simulated ($\approx 10^{11}$ W/cm^2), the Rabi frequency ($\approx 10^{12}$ s^{-1}) is much less than the inverse rate of the phase ($\approx 10^{14}$ s^{-1}). Also for the present analysis, we have in mind experiments where the pulse durations (picoseconds) are much longer than the dephasing times and, consequently, coherent transient effects can be neglected.

For the nondiffusive case, the sum of the population equations [(3) plus (4) plus (5)] equals zero,

$$\Rightarrow N_0 + N_1 = N_T, \tag{7}$$

where the population of the short-lived manifold S_2 is assumed to be negligible due the very short recombination time ($\tau_{12} \sim 0$). The steady-state approximation is employed for the above rate equations such that $\dot{N}_i = 0$. Thus, solving the rate equations above in the steady-state regime, the following nonlinear absorption is obtained:

$$\alpha_{nl} = \alpha_0 \frac{\frac{I}{\hbar\omega}\tau_{01}\sigma_{21} + 1}{\frac{I}{\hbar\omega}\tau_{01}\sigma_{10} + 1}. \tag{8}$$

Therefore, if R is greater than 1 ($\sigma_{21} > \sigma_{10}$), increasing irradiances cause the transmittance to decrease. The irradiance rate equation may now be written

$$\frac{dI(y)}{dy} = -\alpha_0\left[\frac{IR + I_s}{I + I_s}\right]I(y), \tag{9}$$

where a saturation irradiance $I_s = \hbar\omega(\sigma_{10}\tau_{01})^{-1}$ has been defined. Using partial fraction techniques and integrating from 0 to L (material length), the above lends itself to the transcendental solution for transmittance

$$T = \frac{I(L)}{I(0)} = \exp(-\alpha_0 L)\left[\frac{I(L)R + I_s}{I(0) + I_s}\right]^{1 - 1/R}, \tag{10}$$

which is the result for current RSA models.

III. THE ROLE OF STIMULATED EMISSION

Initial excitation promotes electrons into high-lying Franck-Condon states and the molecules typically initiate into vibration, with electrons falling rapidly to the bottom of the S_1 band. In the previous model, the intraband rate was assumed to be zero; however, for sufficiently high irradiances, the influence of stimulated emission from the first-excited-state manifold back to the ground-state manifold cannot be neglected. Indeed, there is a finite intraband vibrational lifetime (τ_v), which, in a sense, controls the extent to which stimulated emission contributes, as shown in Fig. 1(b). The rate equations for this case may be written

$$\dot{N}_0 = -(N_0 - N_1')\sigma_{10}\frac{I}{\hbar\omega} + \frac{N_1}{\tau_{01}} + \frac{N_1'}{\tau_{01}}, \tag{11}$$

$$\dot{N}_1 = -\frac{N_1}{\tau_{01}} + \frac{N_1'}{\tau_v} - N_1\sigma_{21}\frac{I}{\hbar\omega}, \tag{12}$$

$$\dot{N}_1' = (N_0 - N_1')\sigma_{10}\frac{I}{\hbar\omega} - \frac{N_1'}{\tau_{01}} - \frac{N_1'}{\tau_v} - N_1'\sigma_{21}\frac{I}{\hbar\omega} + \frac{N_2}{\tau_{12}}, \tag{13}$$

$$\dot{N}_2 = N_1\sigma_{21}\frac{I}{\hbar\omega} + N_1'\sigma_{21}\frac{I}{\hbar\omega} - \frac{N_2}{\tau_{12}}, \tag{14}$$

$$\frac{1}{c}\frac{\partial I}{\partial t} + \frac{\partial I}{\partial y} = -I[(N_0 - N_1')\sigma_{10} + (N_1 + N_1')\sigma_{21}], \tag{15}$$

where it has been assumed that the absorption cross sections from the upper and lower (N_1' and N_1) S_1 band to the S_2 band are equal. This is a coarse approximation; however, it goes beyond previous approximations. The critical condition for the onset of RSA is too complicated to quote; instead an extreme situation is tested by setting $\tau_v = \infty$. Again if one assumes that $N_2 = 0$, the above may be mathematically manipulated to obtain the resulting transmittance equation
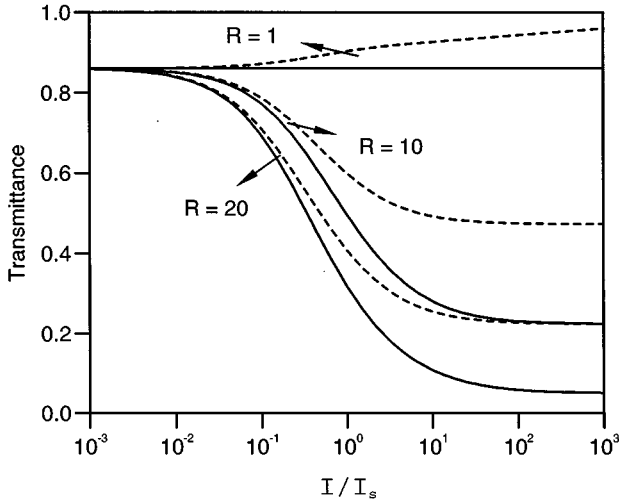
FIG. 2. Simulation of steady-state transmittance against increasing irradiance for a range of $R=\sigma_{21}/\sigma_{10}$ values; also shown is the effect of extreme stimulated emission ($\tau_v=\infty$) depicted by the dashed lines. The linear absorption coefficient $\alpha_0 L$ was chosen to be -0.15.

$$T=\frac{I(L)}{I(0)}=\exp(-\alpha_0 L)\left[\frac{I(L)R+I_s}{I(0)+I_s}\right]^{1-2/R}. \qquad (16)$$

The critical condition is now $R>R_c=2$ as opposed to 1. Thus, with the inclusion of a finite τ_v, the criterion for induced absorption is that R lies between 1 and 2. Figure 2 shows theoretical plots of transmittance against irradiance, in units of saturation irradiance I_s. Plots for various values of R are shown that verify the trend of decreasing transmittance as the ratio of the first-excited-state to ground-state absorption increases. The dashed simulations include the effect of stimulated emission from the S_1 manifold, which for an R value of 1 tends towards bleaching, since the critical condition has been increased to 2. This is caused by the excited-state absorption now having to compete with stimulated emission back to the ground state as well as with the τ_{01} process. To recapitulate, the stimulated emission acts to inhibit the excited-state absorption as is expected from the absorption expression $\alpha_{nl}=(N_0-N_1)\sigma_{10}+N_1\sigma_{21}$.

IV. INCLUSION OF THE SECOND-EXCITED-STATE RECOMBINATION LIFETIME τ_{12}

Previous models [9,2,17,18,4,19] of reverse saturable absorption include the assumption of an infinitesimal second-to first-excited-state interband lifetime. Consequently, the absorption coefficient saturates to a high value as the population in the S_1 manifold begins to dominate. Nevertheless, RSA action may cease when accumulation of population in the second excited state (S_2) depletes the number of molecules contributing to the absorption processes. The detailed behavior will depend on the cross sections and lifetimes of a series of excited states of the material. Utilizing Fig. 1(c), the absorption coefficient becomes

$$\alpha_{nl}=\alpha_0 \frac{\dfrac{I}{I_s R}+1}{\dfrac{I}{I_s}+1+\left(\dfrac{I}{I_s}\right)^2 \dfrac{\tau_{12}}{\tau_{01}}R}, \qquad (17)$$

which yields the transmittance solution

$$T=\exp\left(-\alpha_0 L-\frac{\tau_{12}}{\tau_{10}}\frac{I(L)-I(0)}{I_s}\right)$$
$$\times\left[\frac{I(L)R+I_s}{I(0)+I_s}\right]^{1-1/R+\tau_{12}/\tau_{01}R}. \qquad (18)$$

The criterion for the onset of induced absorption is now

$$R>R_c=\frac{1}{1-\dfrac{I\tau_{12}}{I_s\tau_{01}}}; \qquad (19)$$

i.e., the following must be satisfied:

$$R>1, \qquad (20)$$

$$0<I<I_s\frac{\tau_{01}}{\tau_{12}}\left(1-\frac{1}{R}\right). \qquad (21)$$

This points out that, contrary to earlier suppositions, the critical condition for achieving RSA is actually a function of the radiation parameters and does not depend solely on the material characteristics. Further, the reader should note that there are, in fact, numerous laser dyes that have a significantly greater excited-state absorption cross section to ground-state cross section, but still exhibit saturable absorption. Speisser and Shakkour [22] have measured various photoquenching parameters of numerous saturable dyes that indicate some very high R values; however, these dyes act as saturable absorbers because of their relatively long τ_{12} lifetimes. Theoretically, typical laser parameters with an R value of $\sim$40 and τ_{12} of $\sim$60 ps can show an increase in R_c below an energy of 1 nJ ($I_s\approx10^7$ W cm^{-2}) for picosecond pulses. It seems almost paradoxical that a greater excited-state absorption cross section actually causes the critical condition to increase at lower irradiances since this imposes a limit to the overall dynamic range for induced absorption. These predictions have been confirmed experimentally for picosecond pulses with fluences of the order 0.1 J cm^{-2} [14–16] and will be modeled theoretically in Sec. VI. Figure 3 shows the steady-state RSA responses for various second-excited-state decay lifetimes assuming an R value of 20; with a recombination lifetime τ_{12} of 0.001 ps (solid line), the transmittance saturates to a low value, as expected. However, as τ_{12} is increased to 0.1 ps (dot-dashed line) and 1 ps (dashed line), the dynamic range is seen to be severely restricted for increasing τ_{12} values. Finally, Fig. 4 shows the effect that stimulated emission has on these findings, which again inhibits the induced absorption. For the above simulations, the first-excited-state lifetime τ_{01} was set equal to 1 ns, which is typical of RSA dyes [3,18,23].
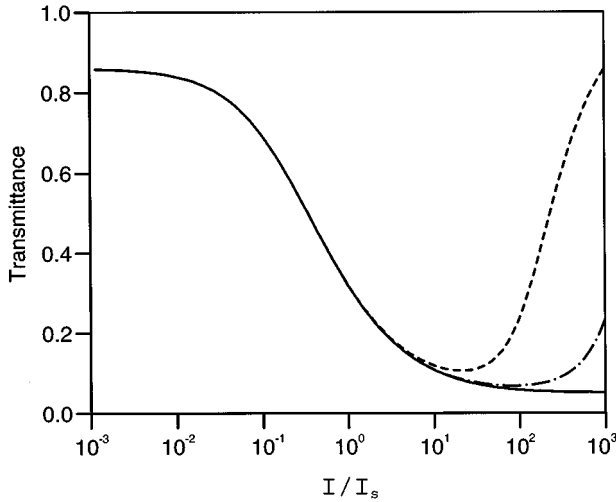
FIG. 3. Steady-state transmittance calculations demonstrating saturation of the excited-state absorption as the recombination time τ_{12} is increased. The first excited-state recombination lifetime τ_{01} was set equal to 1 ns and R was taken to be 20. Calculations for a range of τ_{12} were simulated: 0.001 ps (solid line), 0.1 ps (dot-dashed line), and 1 ps (dashed line). For increasing lifetimes, the dynamic range for optical limiting is seen to be severely restricted, in agreement with recent experimental measurements.

V. THE SECOND-EXCITED-STATE ABSORPTION PROCESS

The above analysis suggests that there is a fundamental limit to the performance of any reverse-saturable dye for sufficiently high irradiances. However, as the S_2 manifold becomes significantly populated, the absorption from this second excited state becomes an important factor in determining the high-fluence response [see Fig. 1(d)]. In particular, this transition will have a key influence on whether the saturation of the excited-state absorption occurs. If one denotes the second-excited-state absorption cross section by σ_{32}, where $\sigma_{32}=R'\sigma_{10}$, then the RSA criterion becomes
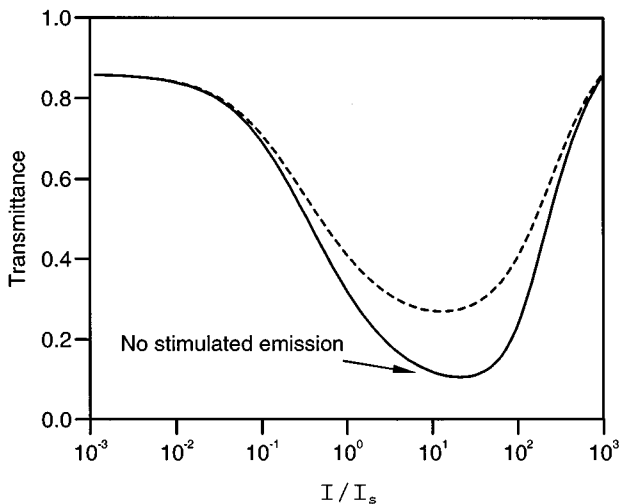
FIG. 4. Influence of stimulated emission (solid to dashed calculations) on the saturation limit response depicted in Fig. 3, where the corresponding R and τ_{12} values were taken to be 20 and 1 ps, respectively.

$$R > R_c = \frac{1 + R'\,\dfrac{\tau_{12}}{\tau_{01}}\,\dfrac{I}{I_s}}{1 + \dfrac{\tau_{12}}{\tau_{01}}(2R'-1)\dfrac{I}{I_s}} ; \tag{22}$$

hence

$$R > 1, \tag{23}$$

$$0 < I < \frac{I_s[1-R]}{R\,\dfrac{\tau_{12}}{\tau_{01}}[2R'-1] - R'\,\dfrac{\tau_{12}}{\tau_{01}}} . \tag{24}$$

Thus, if σ_{32} is sufficiently large, the saturation of the induced absorption may be prevented. As an example, when $\tau_{12}/\tau_{01}=0.001$, $I=10I_s$, and $R'=0.1$, then the critical ratio R_c becomes 5.5; but with $R'=1$, R_c is 1.005.

VI. DYNAMIC SIMULATIONS

To study the interaction of an intense, short-picosecond pulse propagating in a nonlinear medium, ultimately one has to appeal to numerical techniques. To simulate nonlinear optical pulse propagation, the pulse is split into time (δt) and radius (δr) increments, while the sample that exhibits a nonlinear polarization is split into space slices (δy). The task is therefore to calculate the irradiance $I(t_i, r_j, y_k)$, where the subscripts i,j,k represent the various slices. Each irradiance slice experiences the boundary conditions created by the previous time slice, which enables the solution to be obtained iteratively for any multilevel model.

To model pulse propagation our aim is to solve the time-dependent rate equations describing the nonlinear medium, for every slice of the input pulse, and also step it through the sample in order to take account of pulse depletion. The first time slice ($i=1$) approaches the multilevel material with the boundary conditions $N_i=0$ and $N_0=N_T$, where N_i refers to the population in each level. The input irradiances then create excitations that consequently affect the next time slices. In the absence of spatial diffusion, the pulse can either be stepped through the first sample slice with successive time slices, for all radii, and so on to the next sample slice or, alternatively, stepped through the first time slice, at all radii, through the entire sample space slices and repeated for all subsequent time radii slices. Since we calculate all the populations at all times and radii, we can calculate the nonlinear absorption for the entire pulse through the first space slice, which then leads to the next sample slice, where the entire process is repeated. The eventual output irradiances are integrated to obtain the energy and, subsequently, the transmittance. This algorithm allows us to take into account the radial distribution of the dielectric polarization and a possible variation of the pulse shape inside the absorber. The various slices were minimized when a stable solution was approached, i.e., when increasing the slices resulted in approximately the same output. Typically, time slices of 500, radius slices of 25, and sample slices of 10 were found to be sufficient.
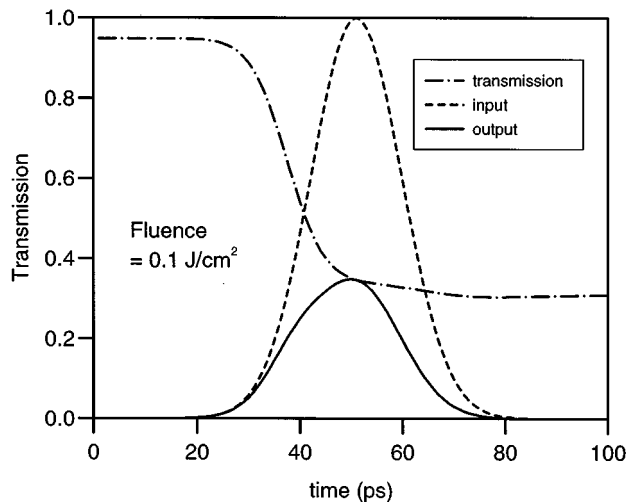
FIG. 5. Dynamical simulations, showing the input and the output pulse, assuming an R value of 30 and $\tau_{12}=0.01$ ps. Also shown is the corresponding transmission as a function of time. The input fluence was 0.1 J cm^{-2}.

For the simulations, known experimental laser and material parameters are used [14]. Pulses of wavelength 532 nm, 15 ps in duration (HW e^{-1} maximum irradiance), and a spot size of 90 μm (HW e^{-2} maximum) were assumed and the nonlinear material was taken to have a 1-mm path length, corresponding to a dye solution with a molecular concentration of 9.5×10^{16} cm^{-3} and a ground-state absorption cross section of 1.67×10^{-17} cm^{2}. These parameters correspond to the experimental measurements to be modeled in Fig. 9.

Figure 5 depicts a single pulse simulation for a peak input fluence of 0.1 J cm^{-2} ($I_0=3.8\times10^{9}$ W cm^{-2}) using the model in Fig. 1(c), which shows the input pulse, the output pulse, and the transmission as a function of time. As can be recognized, the transmission drops for increasing irradiances and consequently the latter half of the pulse-time profile experiences greater absorption. The first-excited-state to ground-state lifetime τ_{01} was taken to be 1.5 ns, resulting in the long recovery of the nonlinear transmittance. The upper excited-state to first-excited-state lifetime τ_{12} was taken to be 0.01 ps and the excited-state absorption cross section was assumed to be 30 times that of the ground-state absorption cross section, i.e., $R=\sigma_{21}/\sigma_{10}=30$. In Fig. 6 the corresponding relative populations of the first three manifolds are shown as a function of time. As can be seen, when the irradiances become high, N_0 starts to decrease, resulting in an increase of the first-excited-manifold population, which eventually dominates due to high irradiances and the long recovery time. Near the center of the pulse, the irradiances are sufficiently high to cause accumulation of the molecules into the second-excited manifold. This point is further emphasized in Fig. 7, where the input fluence has been increased to 10 J cm^{-2} and hence the S_2 manifold becomes significantly populated, temporarily dominating in the high irradiance regime, even for the fast recovery time of 0.01 ps.

From these findings, it is clear that the performance of a RSA dye is influenced by a range of molecular parameters and not just the first-excited recombination lifetime and the
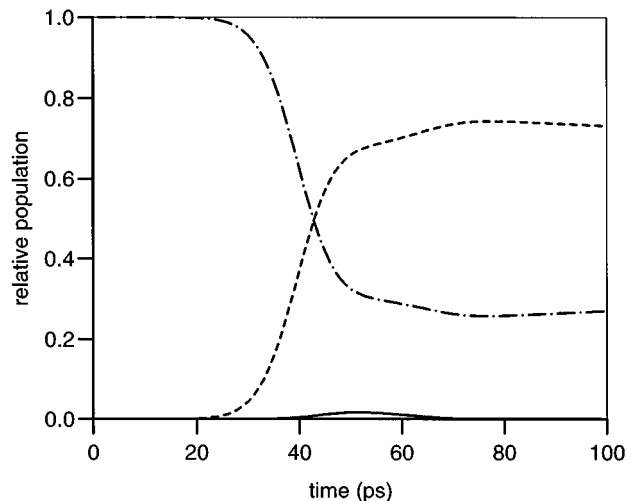
FIG. 6. Dynamical evolution of the first three manifold populations with the molecular parameters as in Fig. 5.

R value as was previously thought. Consequently, general figures of merit are presented here to enhance the dynamic range for induced absorption (power limiting). To prevent the saturation of the excited-state absorption, one should aim to satisfy

$$\frac{\tau_{01}}{\tau_{12}}\gg R, \tag{25}$$

$$R'\gg1, \tag{26}$$

$$\alpha_0 L\gg0, \tag{27}$$

where α_0 is the low irradiance (linear) absorption coefficient and L is the length of the sample. As an example of the above, consider what happens if one varies the value of the interband nonradiative decay τ_{12}: Fig. 8 shows the substantial effect that this excited-state lifetime can have on the
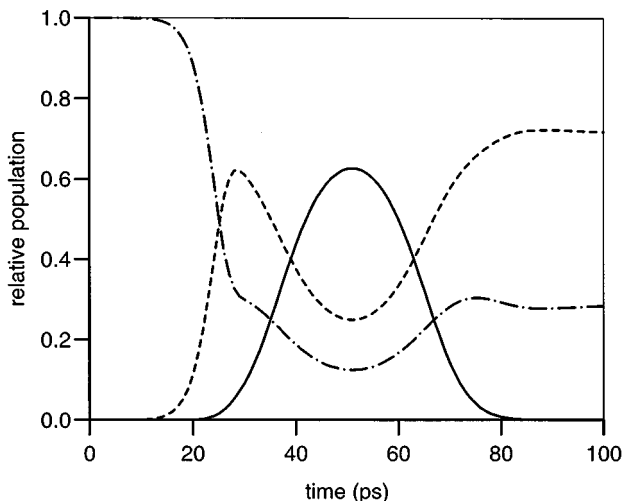
FIG. 7. Same as in Fig. 6, where the fluence has been increased from 0.1 to 10 J cm^{-2}. Consequently, the population in S_2 becomes significant.
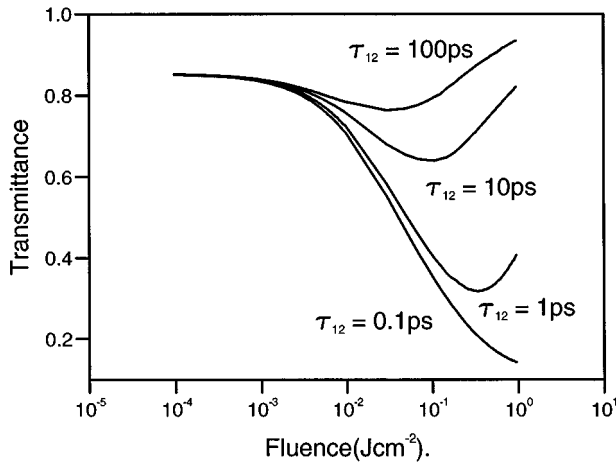
FIG. 8. Picosecond single-pulse transmittance simulations for various values of the upper second to the first excited-state nonradiative decay τ_{12}. It is seen that if τ_{12} ($=1.5$ ns) is sufficiently long, then reverse saturable absorption (induced absorption) is followed by induced transmission for higher fluences.

FIG. 9. Picosecond single-pulse transmittance measurement for HITCI (see the text). Reverse saturable absorption is seen for the lower input fluences and reduction of absorption for higher fluences. Also included are two theoretical simulations: model 1, whose vibrational lifetime is a fast $\tau_v=0.1$ ps, and model 2, which assumes an infinite ($\tau_v=\infty$) intraband relaxation time.

transmittance characteristics, a faster decay being advantageous if high-fluence optical limiting is desired.

As one can see, if the second-excited excitation is small ($R'\ll1$), a necessary condition for taking advantage of a large R value is $\tau_{01}/\tau_{12}\gg R$. Furthermore, lower R values, which still satisfy the critical condition, will produce a greater dynamic range for the induced absorption.

Finally, the theoretical techniques discussed and presented are applied to fit the experimental measurements for the RSA dye, 1,3,3,1′,3′,3′-hexamethylindotricarbocyanine iodide (HITCI) [24–27] as a reverse saturable absorber at 532 nm (for the experimental details, see Ref. [14]).

From single-pulse transmittance measurements (see Fig. 9), an increase in transmittance coefficient at high fluences, following low-fluence reverse saturable absorption (induced absorption), is demonstrated, which allows the extraction of a range of molecular parameters. For example, by fitting, the lifetime of the second excited state is determined to be $\tau_{12}=10$ ps, a lifetime previously assumed to be infinitely fast with respect to the optical pumping rate of the laser.

The model in Fig. 1(b) is employed to explain the observed results. Within model 1 (see Fig. 9), τ_{v2} was set to ≤0.1 ps, which is found to explain the experimental data very well. Model 2 simulates the transmittance with $\tau_v=\infty$, which does not fit the high-fluence data points as well as model 1. In either case, the R value (σ_{21}/σ_{10}) was found to be 29 (±2), in good agreement with the value of 30 determined by Zhu and Harris [26].

It has been proposed that reverse saturable dyes, with their fast response times, could be exploited in optical limiting components [2–4]. However, as predicted theoretically and demonstrated experimentally, once RSA action has set in, it does not necessarily continue to all higher fluences. One finds that the reverse saturable absorption observed at levels of typically 0.01–0.1 J cm^{-2} is itself reversed, leading to absorption recovery and eventually absorption saturation for fluences greater than 2 J cm^{-2}.

VII. CONCLUSION

In conclusion, various rate-equation models were analyzed for reverse saturable absorption in the steady-state and dynamic regimes. The current definition of a RSA dye was discussed (those materials having a larger excited-state cross section than the ground-state cross section) and its limitations were pointed out. The previous definition sounds intuitively correct, at least for a three-level system, and can be derived from the simple absorption equation $\alpha_{nl}=N_0\sigma_{10}+N_1\sigma_{21}$, where the condition for induced absorption is $\alpha_{nl}-\alpha_0>0$. For high irradiances, the above expression was found to be incomplete on two accounts: first, it neglects the inclusion of stimulated emission from the excited-state manifold S_1, and second, the excited-state population N_2 is assumed to be zero and hence the excited-state interband lifetime τ_{12} is taken to be infinitesimal.

With the inclusion of stimulated emission, the critical condition is that R (σ_{21}/σ_{10}) must lie somewhere between 1 and 2 depending on the value of the intraband vibrational lifetime of the S_1 manifold (τ_v). Moreover, it was found that with the inclusion of a finite second-excited-state interband lifetime (τ_{12}), the critical condition for RSA is not fixed but increases with increasing input irradiance. Steady-state and dynamic response curves were simulated to demonstrate the influence of various material and radiation parameters. Finally, the models were applied to fit experimental measurements for the RSA dye HITCI. These results explain recent experimental findings for picosecond pulses and have important implications alone for future exploitation of reverse saturable absorbers in the field of high-fluence optical limiting.

ACKNOWLEDGMENTS

[1] Y. B. Band, in *Proceedings of the Fritz Harz International Symposium* (Plenum, New York, 1985), p. 23.

[2] D. J. Harter, M. L. Shand, and Y. B. Band, J. Appl. Phys. **56**, 865 (1984).

[3] D. R. Coulter, V. M. Miskowski, J. W. Perry, T. Wei, E. W. Van Stryland, and D. J. Hagan, SPIE Proc. **1105**, 42 (1989).

[4] M. P. Joshi, S. R. Mishra, H. S. Rawat, S. C. Mehendale, and K. C. Rustagi, Appl. Phys. Lett. **62**, 1763 (1993).

[5] T. Wei, D. J. Hagan, M. J. Sence, E. W. Van Stryland, J. W. Perry, and D. R. Coulter, Appl. Phys. B **46-51**, 46 (1992).

[6] K. Mansour, D. Alverez Jr, I. Choong, K. J. Perry, S. Marder, and J. W. Perry, in *Proceedings of the International Conference on Lasers and Electro Optics (CLEO)*, Vol II of 1993 OSA Technical Digest Series (Optical Society of America, Washington, D.C., 1993), p. 614.

[7] J. M. Burzler, S. Hughes, and B. S. Wherrett, Appl. Phys. B **62**, 389 (1996).

[8] A. A. Said, T. H. Wei, R. Desalvo, Z. Wang, M. Sheik-Bahae, D. J. Hagan, and E. W. Van Stryland, SPIE Proc. **1692**, 37 (1992).

[9] C. Li, L. Zhang, M. Yang, H. Wang, and Y. Wang, Phys. Rev. A **49**, 1149 (1994).

[10] C. R. Giuliana and L. D. Hess, IEEE J. Quantum Electron. **QE-3**, 357 (1967).

[11] Y. B. Band, Chem. Phys. Lett. **127**, 381 (1986).

[12] W. Blau, H. Byrne, W. M. Dennis, and J. Kelly, Opt. Commun. **56**, 1985 (1993).

[13] T. H. Wei, D. J. Hagan, M. J. Sence, E. W. Van Stryland, J. W. Perry, and D. R. Coulter, Appl. Phys. B **54**, 46 (1992).

[14] S. Hughes, G. Spruce, B. S. Wherrett, K. R. Welford, and A. D. Lloyd, Opt. Commun. **100**, 113 (1993).

[15] S. Hughes, G. Spruce, B. S. Wherrett, and K. R. Welford, in *Proceedings of the International Conference on Lasers and Electro Optics (CLEO)* (Ref. [6]), p. 614.

[16] W. W. Van Stryland *et al.* have also recently observed the phenomenon of saturation of the excited state for a range of RSA dyes (private communication); S. N. R. Swatton, K. R. Welford, S. J. Till, and J. R. Samples, Appl. Phys. Lett. **66**, 1868 (1995).

[17] G. R. Allan, D. R. Labergerie, S. J. Rychnovsky, T. F. Boggess, A. L. Smirl, and L. Tutt, J. Phys. Chem. **96**, 631 (1992).

[18] J. W. Perry, L. R. Khundkar, D. R. Coulter, J. D. Alverez, S. R. Marder, T. Wei, M. Sence, E. W. Van Stryland, and D. Hagan, *Organic Molecules for Nonlinear Optics and Photonics* (Kluwer Academic, Dordrecht, 1991), p. 369.

[19] K. P. J. Reddy, Opt. Quantum Electron. **19**, 203 (1987).

[20] Y. B. Band and R. Bavli, Phys. Rev. A **36**, 3203 (1987).

[21] S. Hughes, J. M Burzler, G. Spruce, and B. S. Wherrett, J. Opt. Soc. Am. B **12**, 1888 (1995).

[22] S. Speiser and N. Shakkour, Appl. Phys. B **38**, 191 (1985).

[23] S. Hughes, B. S. Wherrett, and G. Spruce, J. Opt. Soc. Am. B (to be published).

[24] J. P. Fouassier, D. J. Lougnot, and J. Faure, Opt. Commun. **18**, 263 (1976).

[25] J. Ivra, Z. Burshtein, and E. Miran, Appl. Opt. **30**, 2848 (1991).

[26] X. R. Zhu and J. M. Harris, Chem. Phys. **142**, 301 (1990).

[27] J. Ivra, Z. Burshtein, and E. Miron, Appl. Opt. **30**, 2484 (1991).